
Reusing Overtrained Language Models Saturates Scaling

Seng Pei Liew¹ Takuya Kato¹

Abstract

Reusing pretrained base models for further pre-training, such as continual pretraining or model growth, is promising at reducing the cost of training language models from scratch. However, the effectiveness remains unclear, especially when applied to overtrained base models. In this work, we empirically study the scaling properties of model reuse and find that the scaling efficiency diminishes in a predictable manner: The scaling exponent with respect to second-stage training tokens decreases logarithmically with the number of tokens used to pretrain the base model. The joint dependence on first- and second-stage tokens is accurately modeled by a simple scaling law. Such saturation effect reveals a fundamental trade-off in multi-stage pretraining strategies: the more extensively a base model is pretrained, the less benefit additional pretraining provides. Our findings provide practical insights for efficient language model training and raise important considerations for the reuse of overtrained models.

1. Introduction

Large language models (LLMs) have recently shown astounding performance in various natural language processing tasks, reaching human-level capabilities in some cases (Achiam et al., 2023; Anthropic, 2024; Gemini Team Google, 2023). However, training/pretraining these models from scratch is computationally expensive and time-consuming, requiring weeks to months even with powerful GPU clusters. To address this challenge *within the pre-training stage itself*, researchers have explored strategies for reusing existing pretrained (base) models for various purposes. These include strategies to learn with new pretraining data, or to increase the model size, without starting from scratch. Such strategies, which pretrain a model through multiple stages, are collectively referred to as *model reuse* throughout this paper.

¹SB Intuitions, Tokyo, Japan. Correspondence to: Seng Pei Liew <sengpei.liew@sbintuitions.co.jp>.

More specifically, we are interested in strategies that (1) improve domain-specific performance through *continual pretraining* (CPT) of the base model (see, e.g., Ibrahim et al. (2024)); or (2) scale model capacity via *model growth* techniques, which increase the model size reusing base model parameters to speed up training (Chen et al., 2015). These strategies have been shown to be promising at accelerating performance improvement of language models while reducing computational costs of pretraining from scratch.

On the other hand, when a base model is overtrained, intuitively, its highly optimized parameters make effective exploration after capacity enlargement for model growth (or exploration with new data distribution for CPT) difficult, causing the second stage to learn slower. This is closely related to the loss of plasticity for neural networks over changing tasks (Ash & Adams, 2020; Sodhani et al., 2020; Lyle et al., 2023; 2024). Hence, it is unclear if the second stage of pretraining can be effectively applied to language models that are overtrained.

In this paper, we seek to understand the scaling properties of such methods by running a multitude of controlled language modeling experiments. We find that, from the performance (cross-entropy loss) perspective, reusing overtrained base models leads to *saturation* in scaling during the second-stage pretraining. Specifically, we show that this effect is *quantifiable* via scaling laws: **The scaling exponent (with respect to the number of training tokens in the second stage) decreases as the base model is trained for longer periods of time. The decrease is proportional to the logarithm of the number of training tokens invested to the first stage.** See Figure 1. Our work bears practical implications as even relatively tiny models are overtrained to trillions of tokens nowadays (Zhang et al., 2024b; Dubey et al., 2024), and model reuse strategies are widely adopted.

Summary of contributions. More technically, our key contributions are as follows:

- We conduct extensive experiments on language models of various sizes and pretraining tokens/datasets (with over 450 runs), to study the scaling properties of model reuse methods, including continual pretraining and model growth.
- We find that for a wide range of configuration of these

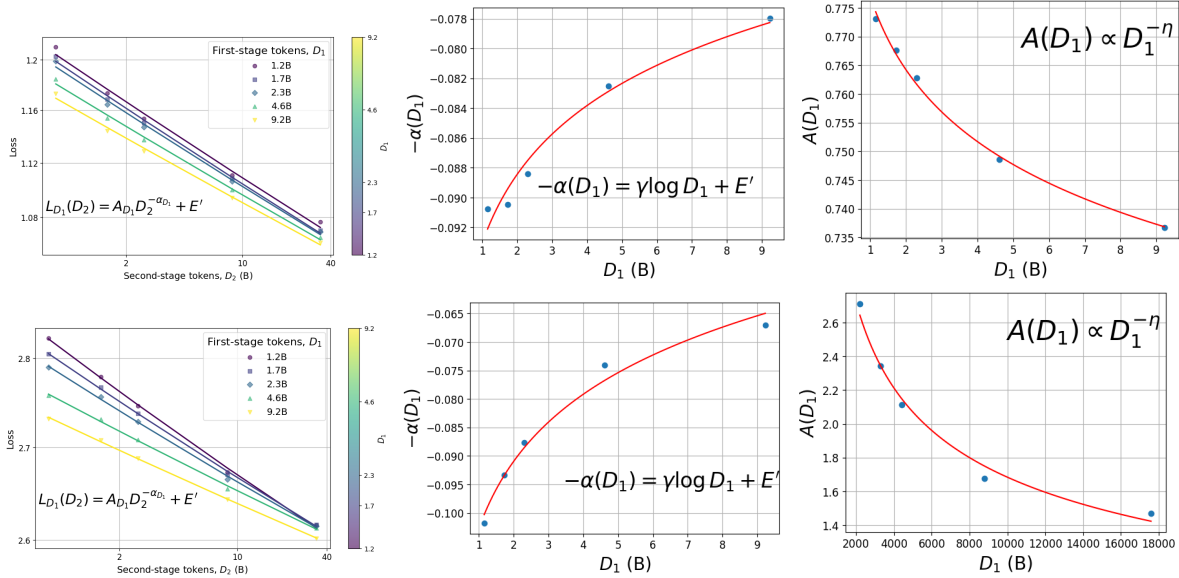


Figure 1. **Model reuse with overtrained base models leads to saturation in scaling behavior.** **Left:** D_2 has power-law scaling. We show scaling behavior of second-stage training tokens (D_2) for different values of first-stage tokens (D_1), trained on a 0.1B base model. **Middle:** Interaction term explains decreasing exponents. The fitted exponents in the left plots are used to fit Equation 3 as a function of D_1 , and are shown to agree well with the functional form. **Right:** Scaling factor has power-law scaling w.r.t. D_1 . **Top:** Continual pretraining (CPT) on code data. **Bottom:** Model growth from 0.1B to 0.2B by stacking.

methods, the following empirical scaling relation holds:

$$L(D_1, D_2) = AD_1^{-\alpha_1} D_2^{-\alpha_2 + \alpha_3 \log D_1} + E \quad (1)$$

where L is the validation loss after the second stage, D_1 and D_2 are the number of training tokens in the first and second stages, respectively, and $A, \alpha_1, \alpha_2, \alpha_3, E$ are positive constants. We denote the term $\alpha_3 \log D_1$ as the *interaction term*. The scaling exponent with respect to D_2 then quantifies the saturation effect of model reuse. We also formulate other plausible functional forms to make comparisons, showing that the above formula still best fits the empirical observation.

- We further analyze the scaling properties with respect to model size, and show that the scaling laws can be extended to jointly incorporate model size together with dataset sizes, see Equation 9. Limitations of our scaling law formulation when training with an extremely large number of tokens are also discussed.
- We demonstrate how the scaling laws can provide guidance on when to train from scratch instead of model reuse to mitigate the negative effects of overtraining. Moreover, we analyze the saturation phenomenon both mechanistically and via a toy model.

Notations used throughout the paper are summarized in Appendix A.

1.1. Related Work

Continual pretraining. CPT has been widely used to adapt existing LLMs to specific domains (Sun et al., 2020; Jang et al., 2022a;b), including code (Yadav et al., 2023; Zan et al., 2022; Guo et al., 2024) and mathematics (Gong et al., 2022; Shao et al., 2024) domains, to be studied in this work. Systematic studies at scale are relatively fewer, and our methodology mainly follows Ibrahim et al. (2024).

Model growth. While Chen et al. (2015) was the first model growth work in the deep learning era, the idea of growing neural networks from smaller ones can be traced to the 90s (Fahlman & LeBiere, 1989; Fahlman, 1990). More recent language model-related model growth methods include Gong et al. (2019); Chen et al. (2021); Wang et al. (2023a;b); Shen et al. (2022); Evci et al. (2022); Yao et al. (2024), which were subsequently systematically analyzed in Du et al. (2024), motivating our choice of model growth methods.

Power-law ansatz. We assume that the final validation loss L follows the widely observed *power-law scaling* with respect to a single variable of interest, such as the number of training tokens or the model size (Hestness et al., 2017; 2019; Henighan et al., 2020):

$$L = AX^{-\alpha} + E, \quad (2)$$

where X is the variable of interest, α is the scaling exponent, A is the scaling factor, and E is the irreducible loss due to

the inherent entropy of the data distribution.¹

Similar to CPT, the reduced capability of transfer learning of code data from models pretrained on natural language data was observed in Hernandez et al. (2021), where the authors denoted as ossification. A similar phenomenon was also observed in the pretraining-fine-tuning pipeline (Springer et al., 2025). These studies however did not quantify the saturated scaling behavior. Previous fine-tuning scaling studies (Mikami et al., 2022; Zhang et al., 2024a; Bethune et al., 2025) did not observe the subtler saturation effects as well, which is perhaps due to the smaller scale (in terms of training tokens) of their experiments.

2. Experiments

2.1. Setup

Model configuration. We consider decoder-only transformers (Vaswani et al., 2017) pretrained with an autoregressive language modeling objective. Our architecture follows LLaMA (Touvron et al., 2023), incorporating refinements such as SwiGLU activation functions (Shazeer, 2020) and rotary position embeddings (Su et al., 2024). We use the LLaMA tokenizer with a vocabulary size of 32,000. Table 2 of Appendix B contains the model configuration used in this paper.

Training configuration. All experiments are conducted using the Megatron-LM library (Shoeybi et al., 2019). We train models in mixed precision (bfloat16) using the AdamW optimizer (Loshchilov et al., 2017), with maximum learning rates tuned separately for each model size. The learning rate follows the *warmup-stable-decay* (WSD) schedule (Bi et al., 2024; Hu et al., 2024), with the final learning rate decayed to one tenth of the peak value. This schedule enables long training runs and facilitates checkpoint reuse for emulating shorter effective training budgets, reducing computational cost. In Appendix C, we also provide an ablation study with the cosine learning rate schedule to show that they achieve similar performance.

We train the models for a number of tokens to at least roughly 200 times the model size in tokens in total (token-to-parameter ratio). Tables 3 and 4 in Appendix summarize the main training configurations. See also Appendix B for further experimental details and Appendix C for training details and evaluation on downstream tasks.

¹ Strictly speaking, we assume the form $L = \frac{A}{(X+1)^\alpha} + E$, which ensures finiteness at $X \rightarrow 0$. However, since in practice $X \gg 1$ (typically 10^6 or more), we approximate it as $L \approx AX^{-\alpha} + E$ for notational simplicity. Moreover, we use the same symbols A , α , and E to denote the scaling factor, exponent, and additive constant, respectively, for notational conveniences when there is no ambiguity, although they may differ across different variables of interest.

Bootstrapped Pretraining

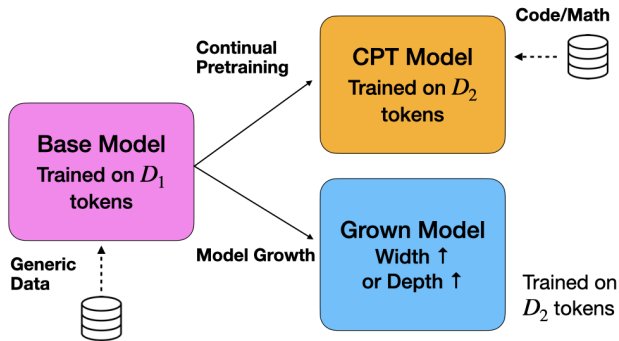


Figure 2. **Illustration of model reuse in consideration.** model reuse consists of two stages: (1) first-stage pretraining of a base model for D_1 tokens on internet/generic data; (2) second-stage pretraining via continual pretraining or model growth for D_2 tokens. Section 3 and 3.2 study and develop scaling laws as a function of these two variables (and additionally model size, N in Section 4) to predict the final loss after the second stage.

Two stages of pretraining. In the context of model reuse, we are primarily interested in how the loss behaves with respect to the number of training tokens used in the two stages of pretraining:

- D_1 : the number of tokens used in the **first-stage** pretraining (base model).
- D_2 : the number of tokens used in the **second-stage** pretraining (CPT or model growth).

Base model. For the first-stage pretraining, we use the CommonCrawl portion of the Slimpajama-DC dataset (Shen et al., 2023), containing 368B tokens in total. The models trained in this stage serve as base checkpoints for the second-stage model reuse experiments.

Continual Pretraining. CPT refers to further training a pretrained model on a large dataset, typically billions of tokens, with the goal of improving performance on a new domain. We distinguish CPT from *instruction tuning*, which typically trains with smaller datasets (millions of tokens or fewer), and is thus harder to analyze the scaling behavior. For our experiments, we perform CPT on the base model with two domain-specific datasets: **Code corpus:** Stack/StarCoder (Li et al.); and **mathematics corpus:** OpenWebMath (Paster et al., 2023). Unless otherwise noted, we adopt the same optimizer and learning rate configurations as the first-stage pretraining.

Model growth. Model growth refers to increasing model capacity by adding new layers and/or expanding hidden

dimensions, thereby increasing the number of trainable parameters. This strategy aims to leverage the representations learned during first-stage training, allowing the larger model to accelerate learning in the second stage. We investigate two model growth techniques shown to be the most effective (in terms of adding new parameters in the width and depth directions) in prior work (Du et al., 2024) (see also Appendix C.5 for more details):

- **Width expansion (exp):** Add new neurons to each layer while using *function-preserving initialization* (FPI), ensuring that the expanded model initially reproduces the behavior of the smaller model.
- **Depth-wise stacking (stk):** Add new layers to the top of the existing one by direct copying, thereby extending model depth.

After performing this procedure, the larger models are trained on the same dataset as the base model. The growth factor is defined as the ratio of the number of non-embedding parameters in the grown model to that in the base model. For both model reuse scenarios in consideration, the validation loss is evaluated on a held-out set from the second-stage dataset. We illustrate the whole framework in Figure 2.

2.2. Experimental Observations

We here provide experimental observations that motivate our formulation of the scaling law. In Figure 1, we show results of training a base model of size 0.1B, and performing CPT on code data, and stacking with a growth factor of 2 on a 5×5 grid of D_1, D_2 .² In the left panels, we plot the second-stage validation loss after the second stage as a function of D_2 for different values of D_1 (left). The following observation is made:

Observation 1: The loss is observed to follow a power law with respect to the number of tokens D_2 , i.e., Equation 2.

This is consistent with previous scaling laws reflecting the expectation that, when starting from a fixed initialization, additional tokens improve performance predictably.

Furthermore, we observe that the fitted scaling exponent of Equation 2 decreases as D_1 increases, with the model growth method more pronouncedly so. To quantify this trend, we express (the minus of) the scaling exponent as a function of D_1 , denoted by $-\alpha(D_1)$. A scatter plot of $-\alpha(D_1)$ reveals a clear logarithmic dependence:

$$-\alpha(D_1) = \gamma \log D_1 + E'. \quad (3)$$

This relationship fits the empirical data well, as shown in the same Figure. Substituting Equation 3 into Equation 2,

²We double the number of non-embedding layers for stacking.

we arrive at a term of the form $D_2^{-E'+\gamma \log D_1}$. Additionally in the same Figure, we show that the multiplicative dependence, $A \propto D_1^{-\alpha_1}$, also holds well. These lead to the following observation:

Observation 2: The dependencies of the second-stage loss jointly on D_1 and D_2 can be captured by a multiplicative scaling law with an interaction term, i.e., Equation 1.

Interpreting the scaling law. Several insights can be made from the scaling law. Fixing D_1 , the effective scaling factor for D_2 becomes $AD_1^{-\alpha_1}$. As D_1 increases, this factor decreases, resulting in a lower initial loss at the start of second-stage pretraining, agreeing with the conventional wisdom that better-pretrained base models (larger D_1) provide stronger initialization for second-stage pretraining.

However, also at fixed D_1 , the effective scaling exponent with respect to D_2 is given by $\alpha_2 - \alpha_3 \log D_1$. This implies that as the base model becomes more overtrained (i.e., larger D_1), the improvement in loss from additional second-stage tokens becomes increasingly marginal. In other words, the returns from increasing D_2 diminish, manifesting as saturation effects at higher D_1 .

3. Scaling Laws for Model Reuse

3.1. Functional Forms for the Scaling Laws

The observations from the previous Section regarding the functional form of the scaling law are purely empirical, which naturally raises the question of whether other functional forms might also fit the observed data. To explore these possibilities, we first derive functional forms that satisfy certain reasonable assumptions, and later fit and compare them empirically with our experimental results.

To recite, our goal is to find a functional form $L(D_1, D_2)$ that captures how the second-stage loss depends jointly on both stages. To derive a principled formulation, we impose two natural constraints:

Condition 1: For a fixed base model trained on D_1 tokens, the second-stage loss should follow a power law with respect to the number of tokens D_2 :

$$L(D_1, D_2) = L_{D_1}(D_2) = A_{D_1} D_2^{-\alpha_{D_1}} + E_{D_1}. \quad (4)$$

This is consistent with classical neural scaling laws and Observation 1. It reflects the expectation that, when starting from a fixed initialization, additional tokens improve performance predictably.

Condition 2: For any fixed value of D_2 , the loss should exhibit power-law behavior with respect to the number of first-stage tokens D_1 :

$$L(D_1, D_2) = L_{D_2}(D_1) = A_{D_2} D_1^{-\alpha_{D_2}} + E_{D_2} \quad (5)$$

This is consistent with the power-law ansatz and captures the intuition that a better-trained base model (i.e., larger D_1) should result in lower loss.

Moreover, this condition implies that as $D_2 \rightarrow 0$, the loss should continuously approach that of the base model: $\lim_{D_2 \rightarrow 0} L(D_1, D_2) = AD_1^{-\alpha} + E$ (as in Footnote 1, we omit the $+1$ term in $D+1$ expressions for notational simplicity, such that terms proportional to D_2 are finite as $D_2 \rightarrow 0$), which is a natural requirement for *function-preserving model growth*; when model capacity is expanded but initialized carefully, the initial loss should remain close to the base model’s loss. We further validate this Condition by showing empirically that the loss follows a power law with respect to D_1 for fixed D_2 in Appendix D.

Together, these conditions lead to the following candidate formulations that jointly satisfy both requirements:

Multiplicative: $L(D_1, D_2) = AD_1^{-\alpha_1} D_2^{-\alpha_2 + \alpha_3 \log D_1} + E.$ (6)

Additive: $L(D_1, D_2) = AD_1^{-\alpha_1} + FD_2^{-\alpha_2} + E.$ (7)

Hybrid: $L(D_1, D_2) = (AD_1^{-\alpha_1} + F)D_2^{-\alpha_2} + E.$ (8)

Note that since $D_1^{-\alpha_1} D_2^{-\alpha_2 + \alpha_3 \log D_1} = D_1^{-\alpha_2 + \alpha_3 \log D_2} D_2^{-\alpha_2}$, the multiplicative form with an interaction term satisfies our conditions, while other forms do not have such an interaction term. We further note that multiplicative scaling laws have been observed in Mikami et al. (2022); Zhang et al. (2024a) but without the interaction term. Liew et al. (2025) empirically showed that sparse upcycling (training sparse mixture-of-experts (MoE) models reusing existing dense models) follows a scaling law similar to Equation 6 but under different motivation and conditions. Our work directly extends their findings to other pretraining paradigms. Equation 8 has also been studied in Barnett (2024).

3.2. Fitting Scaling Laws

To determine the functional form described in the previous Section that best describes the scaling behavior of model reuse methods, we consider a variety of datasets and methods beyond those described in the previous Section.

CPT. We consider both code and mathematics datasets and perform CPT on them as in the previous Section. Additionally, we consider the following variants of CPT that are commonly used in practice (Ibrahim et al., 2024) and test them on the code dataset:

- **CPT with replay (rep):** A portion of the first-stage data is mixed into the second-stage data, which is common for

mitigating catastrophic forgetting. We consider a replay ratio of 0.25, i.e., 25% of the second-stage data is from the first stage.

- **CPT from stable phase (sta):** We consider CPT starting from a base model checkpoint in the stable phase of the WSD learning rate schedule. This is to avoid adverse effects from re-warming the learning rate from a decayed value.

Model growth. In addition to depth-wise stacking described in the previous Section, we consider width expansion that double the size of the base model. For a growth factor of 2, we increase the size of the hidden dimension by $\sqrt{2}$ for width expansion. We further consider stacking variants:

- **Larger growth factor (x4):** We consider a larger growth factor of 4 times (instead of 2).
- **Model growth from stable phase (sta):** Similar to CPT, we train the stacked model starting from a base model checkpoint in the stable phase.

Comparing various functional forms. Running the experiments as described above and obtaining the results, we fit the losses with the functional forms of Equations 6, 7, and 8. Following Hoffmann et al. (2022); Besiroglu et al. (2024), we perform optimization using the Huber loss ($\delta = 10^{-3}$) and the BFGS algorithm, to fit the logarithm of the loss via the LogSumExp trick applied to the RHS of functional forms. The leave-one-out root mean square error (RMS) serves as the goodness-of-fit metric.

As can be seen in Table 1, the multiplicative form with interaction consistently achieves the lowest error across all methods and datasets, indicating that it best captures the underlying scaling behavior. To visualize these relationships, we compare the loss-versus-token plots of our proposed scaling law against alternative functional forms (Figure 3, left panel), using a 0.5B-to-1B model by stacking. The predicted losses from the alternative forms are visually confirmed to fit the empirical data worse. More importantly, the predicted losses from alternative forms with varying D_1 remain nearly parallel across the range of D_2 , whereas ours converges, a distinct behavior that is not captured by other forms. In Appendix D.2, we compare with yet another scaling formulation (“continuous” scaling law (Que et al., 2024; Tissue et al., 2024)) and show that our scaling law still fits better.

Overall, the proposed scaling law is robust across datasets, configurations, and methods investigated. While we acknowledge the possibility of edge cases that deviate from this law, it is important to note that our empirical validation specifically targeted training methodologies that are considered scalable and representative of current best practices

Table 1. **Multiplicative scaling law with interaction consistently achieves lowest error.** Leave-one-out RMS error ($\times 10^{-3}$) for fitting the loss for model reuse of a 0.1B base model. Functional forms are from Equations 6 (and the specific case where $\alpha_3 = 0$), 7, and 8.

RMS ($\times 10^{-3}$)	Code	Math	CPT (rep)	CPT (sta)	Exp x2	Stk x2	Stk x4	Stk (sta)
Mul.	1.573	1.737	0.987	1.371	2.790	2.845	2.152	2.957
Mul. ($\alpha_3 = 0$)	2.095	3.147	2.222	2.366	4.837	7.818	6.557	8.757
Add.	3.913	7.443	4.646	4.315	9.855	10.323	8.866	10.559
Hyb.	2.245	3.340	2.223	2.367	4.841	7.748	6.667	8.822

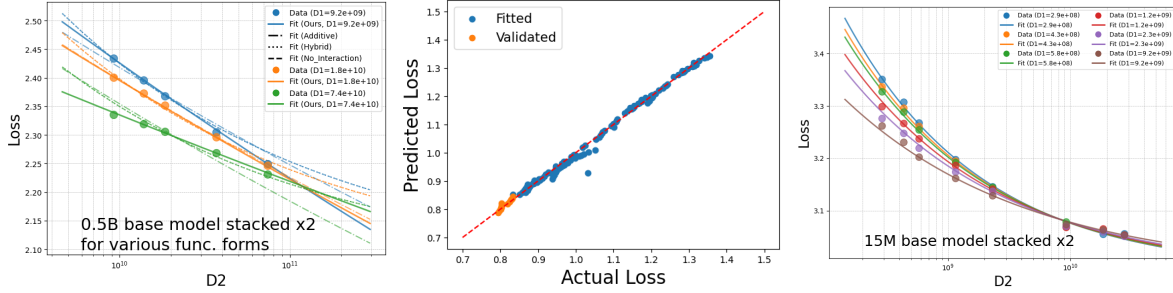


Figure 3. **Left: Visual comparison of various functional forms.** We show scaling behavior of second-stage training tokens (D_2) for different values of first-stage tokens (D_1) for model growth by stacking (growth factor 2, 0.5B-to-1B model), comparing various functional forms. Our proposed multiplicative scaling law with interaction (solid lines) fits the data (dots) best, and lines with different D_1 cross over, indicating saturation effects. Note that the hybrid functional form (dotted lines) nearly overlaps with the multiplicative without interaction form (dashed lines) in this plot. **Middle: Joint scaling law fit for continual pretraining on code data.** Orange points indicate the 10% of data with lowest losses used for validation. **Right: Stacking with extremely large token-to-parameter ratio.** At the limit of large token (D_2)-to-parameter ratio, the values of the loss are too noisy to yield a definite characterization of the crossover region.

in the field. Consequently, we conclude that the scaling behavior and saturation effect identified here are not isolated phenomena, but are fundamentally representative of general model reuse methods employed in efficient LLM development.

4. Extensions and Limitations

4.1. Joint Scaling Incorporating Model Size

We proceed to extend the data scaling law to include model size, N . Let us first focus on CPT where the model size remains unchanged after second-stage pretraining. To determine the functional form, we impose that the loss follows the well-grounded ‘‘Chinchilla’’ scaling law (Hoffmann et al., 2022) (which jointly models the base model’s loss with respect to dataset and model sizes) with respect to D_2 and N .

Condition 3: For a fixed base model trained on D_1 tokens, the second-stage loss should follow the Chinchilla scaling law with respect to the number of tokens D_2 and model size N :

$$L_{D_1}(D_2, N) = A_{D_1} D_2^{-\alpha_{D_1}} + N_{D_1}^{-\beta_{D_1}} + E_{D_1}.$$

The straightforward functional form that satisfies the

Chinchilla-style scaling law is:

$$L(D_1, D_2, N) = A D_1^{-\alpha_1} D_2^{-\alpha_2 + \alpha_3 \log D_1} + B N^{-\beta} + E, \quad (9)$$

which is also consistent with the conditions (power-law ansatz) imposed in Section 3.

Fitting the joint scaling law. We conduct experiments with base models of sizes 15 million (M), 44M, 0.1B, 0.2B, 0.5B and 1B, training them with different numbers of first and second-stage tokens as in Section 3.2. To fit the joint scaling law, we use the same fitting procedure as in Section 3.2, additionally taking N as an additional variable. In the left panel of Figure 4, we show that the formula fits the data well for CPT on code. See Table 7 in Appendix D.3 for the fitted coefficients. In the same Appendix, we further extend our results to model growth where model sizes increase.

The joint scaling law allows us to extrapolate performance to models and datasets larger than those studied experimentally (Figure 3, middle panel). We show in Appendix E.1 with a specific example how it can be used to predict the performance of larger models and datasets. We can further study the compute optimality of CPT and model growth using the joint scaling law, as shown in Appendix E.2.

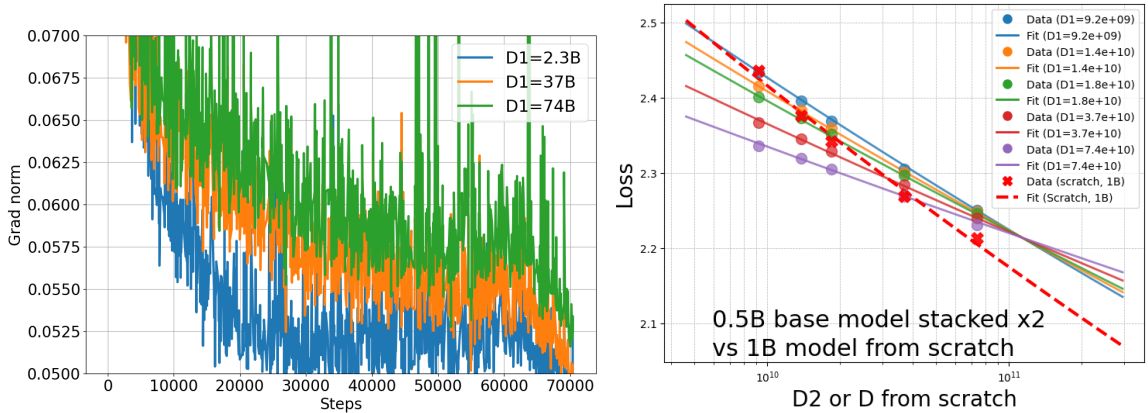


Figure 4. **Left: Overtrained models have larger gradient norms when undergoing model reuse.** We show the gradient norm curves for continual pretraining on code data (1B model) with respect to number of training steps in the second stage for base models trained with different values of first-stage tokens (D_1). We see that overtrained models have larger gradient norms, indicating that the optimization difficulty increases with D_1 , which may explain the saturation effect observed in the scaling law. See Appendix E.4 for model growth results, where similar trends are observed. **Right: Loss versus second-stage (from-scratch) training token for stacking (training from scratch) a 0.5B-to-1B model (1B model).** Data points and fitted lines using our multiplicative scaling law with different number of first-stage training tokens (power-law) are shown. It can be seen that as the number of training tokens increases, the losses from model growth saturate, and from-scratch training eventually outperforms it.

4.2. Limitations of the Scaling Law

We discuss scenarios where our scaling laws may not hold, especially when the number of training tokens is extremely large.

Large D_1 limit. A theoretical limitation of Equation 1 is that as D_1 increases, the effective scaling exponent for D_2 , $\alpha_{\text{eff}} = \alpha_2 - \alpha_3 \log D_1$, decreases without bound, potentially becoming negative when $D_1 > e^{\alpha_2/\alpha_3}$. However, based on our fitted coefficients where α_2 often exceeds α_3 by at least an order of magnitude (see Table 7 in Appendix D.3), this theoretical threshold (e.g., $D_1 > 10^{17}$) is unlikely to be reached in practice. We anticipate the scaling law would break down well before this point.

Alternatively, one can formally model this inevitable thresholding behavior, which marks a deviation from the core power-law ansatz. We propose a modification motivated by Clark et al. (2022) (used for MoE scaling laws): In Equation 1, we replace D_1 with a saturated form, \hat{D}_1 , defined as

$$\hat{D}_1 = (D_1^{-1} + D_{\text{max}}^{-1})^{-1}, \quad (10)$$

where $D_{\text{max}} (\lesssim e^{\alpha_2/\alpha_3})$ is a constant representing the maximum effective number of tokens that can be learned from the first stage. This modification is designed such that when $D_1 \gg D_{\text{max}}$, \hat{D}_1 saturates to D_{max} , preventing unbounded growth of the effective exponent.

Large D_2 limit. Our scaling laws predict that base models trained with different number of tokens in the first stage (D_1) will converge at some point, and diverge again afterwards, with smaller D_1 models performing better at large

D_2 . To see if the latter occurs (under reasonable compute constraints), we train a 15M model with different D_1 values, stack them with growth factor 2, and continue training with extremely large number of tokens in terms of token-to-parameter ratio (up to around a factor of 2000); see Figure 3, right panel.

However, we find that we effectively enter a noise floor at such limits, where stochastic noise can dominate the results. To disentangle such effects, we decay the checkpoints multiple times with different random seeds to estimate the noise variance (details in Appendix E.3). Despite these measures, the data remained too noisy to yield a definitive conclusion regarding the post-crossover regime. We also do not observe crossover for a larger 0.5B-to-1B model; see Appendix E.3. In summary, while our scaling laws predict a crossover, we do not yet find clear empirical evidence that they hold once this point is passed. Given the noise and the exponentially larger compute required to explore this territory, we leave this significantly more compute-intensive study as an open problem.

5. Towards Understanding and Mitigating the Saturation Effects

5.1. Mechanistic Causes

To understand the optimization dynamics of overtrained models, we analyze gradient norms during the second stage of pretraining. We show in the left panel of Figure 4 the gradient norm curves of overtrained and well-trained models

during model reuse. We find that overtrained models exhibit larger gradient norms generally, providing a form of mechanistic explanation for the saturation phenomenon. This aligns with some previous findings (Klein et al., 2024), and also aligns with our initial intuition that the over-optimized parameters are situated in a highly steep/sensitive part of the parameter space relative to the second-stage training, making further optimization difficult. We have also investigated other possible observables but do not find strong correlation with overtraining; see Appendix E.4.

5.2. Practical Mitigation Strategy

Regularization techniques like gradient clipping and layer normalization, are effective at controlling gradient norms, which could potentially mitigate saturation effects. However, such techniques are already employed in our models. Instead of pursuing further optimization or architecture modifications, which may be impractical due to the complexity of large-scale training of language models, we adopt a **direct, data-driven approach**: leveraging the derived scaling laws for both second-stage and from-scratch pretraining to guide practitioners in minimizing the negative effects of overtraining. We specifically target the stacking-based model growth scenario, as it exhibits more serious saturation effects and training from scratch is a common practical alternative.

Denote $L_{2N}^{\text{scratch}}(D)$ by the loss of a model of size $2N$ trained from scratch for D tokens, and $L_N^{\text{growth}}(D_1, D_2)$ by the loss of a model of size $2N$ grown from a base model of size N trained for D_1 tokens, and then trained for D_2 tokens.

In Figure 4 (left panel), we show the plots of the two losses, $L_N^{\text{growth}}(D_1, D_2)$, $L_{2N}^{\text{scratch}}(D)$ with $D = D_2$, using our experimental data as well as the fitted scaling laws for 0.5B-to-1B grown model and from-scratch 1B model training. We see that for small D values, model growth outperforms from-scratch training for all D_1 values considered. However, as D increases, the losses from model growth saturate, and from-scratch training eventually outperforms it. Consequently, the optimal choice between model growth and from-scratch training depends directly on the initial investment (D_1) and the total target training tokens (D_2 or D). This analysis provides a simple, scaling-law-based strategy for practitioners to avoid the negative consequences of reusing overtrained base models.

5.3. A Toy Model

Our previous results are mainly observational and we are unaware of existing theories (Bahri et al., 2024; Paquette et al., 2024; Maloney et al., 2022) that can directly explain why the second-stage scaling exponent decreases logarith-

mically with D_1 . We henceforth take an alternative view by proposing a minimal toy setup in which the logarithmic saturation of the scaling exponent emerges, drawing on the work of learning curve theory (Hutter, 2021), maximum entropy principle (Mandelbrot et al., 1953; Jaynes, 1957a;b), and power-law assumptions. Detailed derivations are relegated to Appendix E.5.

We model the feature space (of infinite dimension) as a k -ary tree with branching factor k . Each datum consists of a single feature, and correct learning of a feature requires observing it once (Hutter, 2021). The rank r of a feature at depth d is approximately $r \approx k^d$. We assume the cost of learning a feature at depth d is proportional to $d \approx \frac{\log r}{\log k}$. Then, following maximum entropy principle, the probability of finding a feature at depth d decays exponentially ($\lambda > 0$ is a constant):

$$P(d) \propto e^{-\lambda d} \propto r^{-\left(\frac{\lambda}{\log k}\right)},$$

establishing that the power-law exponent is $\alpha = \frac{\lambda}{\log k}$.

Hutter (2021) showed that if the data distribution follows power law with exponent $\alpha + 1$, then the overall learning curve also follows a power law with exponent α for small α 's. This sets the exponent of learning with D_2 . To model the effect of D_1 , we posit that first-stage pretraining uncovers more features, effectively expanding the effective branching factor k by a power law: $k_{\text{new}} \approx k \cdot D_1^\delta$, where $\delta > 0$ is a constant. Then, the new exponent becomes

$$\alpha_{\text{new}} \approx \frac{\lambda}{\log k + \delta \log D_1} \approx \alpha - \theta \log D_1,$$

with $\theta = \frac{\lambda \delta}{(\log k)^2}$. We have thus shown (in a minimal setup) that saturation in the scaling exponent can emerge from a tree model with its branching factor modified by first-stage training.

6. Conclusion

We have provided a fairly broad scaling study of two-stage pretraining and there are other potential future directions worth diving deeper into, besides the ones we preliminarily studied in the main text (post-crossover region, mechanistic explanation, theory for saturated scaling): (1) Incorporating other factors into the scaling laws, e.g., replay ratio (Que et al., 2024; Wang et al., 2025) and the growth factor in model growth (Du et al., 2024). (2) Developing more advanced and scalable techniques to completely eliminate saturation effects, complementing the scaling-law-based guidelines presented in this paper.

Impact Statement

This paper works toward the goal of advancing the field of machine learning and language modeling, with an emphasis

on scaling. There are many potential societal consequences of our work, none which we feel must be specifically highlighted here.

References

- Achiam, J., Adler, S., Agarwal, S., Ahmad, L., Akkaya, I., Aleman, F. L., Almeida, D., Altenschmidt, J., Altman, S., Anadkat, S., et al. Gpt-4 technical report. *arXiv preprint arXiv:2303.08774*, 2023.
- Anthropic. Introducing the next generation of claude, 2024. URL <https://www.anthropic.com/news/claude-3-family>.
- Ash, J. and Adams, R. P. On warm-starting neural network training. *Advances in neural information processing systems*, 33:3884–3894, 2020.
- Bahri, Y., Dyer, E., Kaplan, J., Lee, J., and Sharma, U. Explaining neural scaling laws. *Proceedings of the National Academy of Sciences*, 121(27):e2311878121, 2024.
- Barnett, M. An empirical study of scaling laws for transfer. *arXiv preprint arXiv:2408.16947*, 2024.
- Besiroglu, T., Erdil, E., Barnett, M., and You, J. Chinchilla scaling: A replication attempt. *arXiv preprint arXiv:2404.10102*, 2024.
- Bethune, L., Grangier, D., Busbridge, D., Gualdoni, E., Cuturi, M., and Ablin, P. Scaling laws for forgetting during finetuning with pretraining data injection. *arXiv preprint arXiv:2502.06042*, 2025.
- Bi, X., Chen, D., Chen, G., Chen, S., Dai, D., Deng, C., Ding, H., Dong, K., Du, Q., Fu, Z., et al. Deepseek llm: Scaling open-source language models with longtermism. *arXiv preprint arXiv:2401.02954*, 2024.
- Biderman, S., Schoelkopf, H., Anthony, Q. G., Bradley, H., O’Brien, K., Hallahan, E., Khan, M. A., Purohit, S., Prashanth, U. S., Raff, E., et al. Pythia: A suite for analyzing large language models across training and scaling. In *International Conference on Machine Learning*, pp. 2397–2430. PMLR, 2023.
- Bisk, Y., Zellers, R., Gao, J., Choi, Y., et al. Piqa: Reasoning about physical commonsense in natural language. In *Proceedings of the AAAI Conference on Artificial Intelligence*, volume 34, pp. 7432–7439, 2020.
- Chen, C., Yin, Y., Shang, L., Jiang, X., Qin, Y., Wang, F., Wang, Z., Chen, X., Liu, Z., and Liu, Q. bert2bert: Towards reusable pretrained language models. *arXiv preprint arXiv:2110.07143*, 2021.
- Chen, T., Goodfellow, I., and Shlens, J. Net2net: Accelerating learning via knowledge transfer. *arXiv preprint arXiv:1511.05641*, 2015.
- Clark, A., de Las Casas, D., Guy, A., Mensch, A., Paganini, M., Hoffmann, J., Damoc, B., Hechtman, B., Cai, T., Borgeaud, S., et al. Unified scaling laws for routed language models. pp. 4057–4086. PMLR, 2022.
- Clark, P., Cowhey, I., Etzioni, O., Khot, T., Sabharwal, A., Schoenick, C., and Tafjord, O. Think you have solved question answering? try arc, the ai2 reasoning challenge. *arXiv preprint arXiv:1803.05457*, 2018.
- Clauset, A., Shalizi, C. R., and Newman, M. E. Power-law distributions in empirical data. *SIAM review*, 51(4): 661–703, 2009.
- Dao, T., Fu, D., Ermon, S., Rudra, A., and Ré, C. Flashattention: Fast and memory-efficient exact attention with io-awareness. *Advances in Neural Information Processing Systems*, 35:16344–16359, 2022.
- Du, W., Luo, T., Qiu, Z., Huang, Z., Shen, Y., Cheng, R., Guo, Y., and Fu, J. Stacking your transformers: A closer look at model growth for efficient llm pre-training. *arXiv preprint arXiv:2405.15319*, 2024.
- Dubey, A., Jauhri, A., Pandey, A., Kadian, A., Al-Dahle, A., Letman, A., Mathur, A., Schelten, A., Yang, A., Fan, A., et al. The llama 3 herd of models. *arXiv preprint arXiv:2407.21783*, 2024.
- Evcı, U., van Merriënboer, B., Unterthiner, T., Vladymyrov, M., and Pedregosa, F. Gradmax: Growing neural networks using gradient information. *arXiv preprint arXiv:2201.05125*, 2022.
- Fahlman, S. and Lebiere, C. The cascade-correlation learning architecture. In Touretzky, D. (ed.), *Advances in Neural Information Processing Systems*, volume 2. Morgan-Kaufmann, 1989. URL https://proceedings.neurips.cc/paper_files/paper/1989/file/69adc1e107f7f7d035d7baf04342e1ca-Paper.pdf.
- Fahlman, S. E. The recurrent cascade-correlation architecture. In *Neural Information Processing Systems*, 1990. URL <https://api.semanticscholar.org/CorpusID:15720720>.
- Gao, L., Tow, J., Abbasi, B., Biderman, S., Black, S., DiPofi, A., Foster, C., Golding, L., Hsu, J., Le Noac’h, A., Li, H., McDonnell, K., Muennighoff, N., Ociepa, C., Phang, J., Reynolds, L., Schoelkopf, H., Skowron, A., Sutawika, L., Tang, E., Thite, A., Wang, B., Wang, K., and Zou, A. A framework for few-shot language model evaluation,

- 07 2024. URL <https://zenodo.org/records/12608602>.
- Gemini Team Google. Gemini: A family of highly capable multimodal models. *arXiv preprint arXiv:2312.11805*, 2023.
- Gong, L., He, D., Li, Z., Qin, T., Wang, L., and Liu, T. Efficient training of bert by progressively stacking. In *International conference on machine learning*, pp. 2337–2346. PMLR, 2019.
- Gong, Z., Zhou, K., Zhao, X., Sha, J., Wang, S., and Wen, J.-R. Continual pre-training of language models for math problem understanding with syntax-aware memory network, 2022. URL <https://aclanthology.org/2022.acl-long.408/>.
- Guo, D., Zhu, Q., Yang, D., Xie, Z., Dong, K., Zhang, W., Chen, G., Bi, X., Wu, Y., Li, Y., et al. Deepseek-coder: When the large language model meets programming—the rise of code intelligence. *arXiv preprint arXiv:2401.14196*, 2024.
- Hägele, A., Bakouch, E., Kosson, A., Von Werra, L., Jaggi, M., et al. Scaling laws and compute-optimal training beyond fixed training durations. *Advances in Neural Information Processing Systems*, 37:76232–76264, 2024.
- Henighan, T., Kaplan, J., Katz, M., Chen, M., Hesse, C., Jackson, J., Jun, H., Brown, T. B., Dhariwal, P., Gray, S., et al. Scaling laws for autoregressive generative modeling. *arXiv preprint arXiv:2010.14701*, 2020.
- Hernandez, D., Kaplan, J., Henighan, T., and McCandlish, S. Scaling laws for transfer. *arXiv preprint arXiv:2102.01293*, 2021.
- Hestness, J., Narang, S., Ardalani, N., Damos, G., Jun, H., Kianinejad, H., Patwary, M. M. A., Yang, Y., and Zhou, Y. Deep learning scaling is predictable, empirically. *arXiv preprint arXiv:1712.00409*, 2017.
- Hestness, J., Ardalani, N., and Damos, G. Beyond human-level accuracy: Computational challenges in deep learning. pp. 1–14, 2019.
- Hoffmann, J., Borgeaud, S., Mensch, A., Buchatskaya, E., Cai, T., Rutherford, E., de Las Casas, D., Hendricks, L. A., Welbl, J., Clark, A., et al. Training compute-optimal large language models. *Proceedings of the 36th International Conference on Neural Information Processing Systems*, pp. 30016–30030, 2022.
- Hu, S., Tu, Y., Han, X., He, C., Cui, G., Long, X., Zheng, Z., Fang, Y., Huang, Y., Zhao, W., et al. Minicpm: Unveiling the potential of small language models with scalable training strategies. *arXiv preprint arXiv:2404.06395*, 2024.
- Huang, S., Cheng, T., Liu, J. K., Xu, W., Hao, J., Song, L., Xu, Y., Yang, J., Liu, J., Zhang, C., et al. Opencoder: The open cookbook for top-tier code large language models. In *Proceedings of the 63rd Annual Meeting of the Association for Computational Linguistics (Volume 1: Long Papers)*, pp. 33167–33193, 2025.
- Hutter, M. Learning curve theory. *arXiv preprint arXiv:2102.04074*, 2021.
- Ibrahim, A., Thérien, B., Gupta, K., Richter, M. L., Anthony, Q. G., Belilovsky, E., Lesort, T., and Rish, I. Simple and scalable strategies to continually pre-train large language models. *Transactions on Machine Learning Research*, 2024.
- Jang, J., Ye, S., Lee, C., Yang, S., Shin, J., Han, J., Kim, G., and Seo, M. Temporalwiki: A lifelong benchmark for training and evaluating ever-evolving language models. In Goldberg, Y., Kozareva, Z., and Zhang, Y. (eds.), *Proceedings of the 2022 Conference on Empirical Methods in Natural Language Processing, EMNLP 2022, Abu Dhabi, United Arab Emirates, December 7-11, 2022*, pp. 6237–6250. Association for Computational Linguistics, 2022a. URL <https://doi.org/10.18653/v1/2022.emnlp-main.418>.
- Jang, J., Ye, S., Yang, S., Shin, J., Han, J., Kim, G., Choi, S. J., and Seo, M. Towards continual knowledge learning of language models. In *The Tenth International Conference on Learning Representations, ICLR 2022, Virtual Event, April 25-29, 2022*. OpenReview.net, 2022b. URL <https://openreview.net/forum?id=vfsRB5MImo9>.
- Jaynes, E. T. Information theory and statistical mechanics. *Physical review*, 106(4):620, 1957a.
- Jaynes, E. T. Information theory and statistical mechanics. ii. *Physical review*, 108(2):171, 1957b.
- Kaplan, J., McCandlish, S., Henighan, T., Brown, T. B., Chess, B., Child, R., Gray, S., Radford, A., Wu, J., and Amodei, D. Scaling laws for neural language models. *arXiv preprint arXiv:2001.08361*, 2020.
- Klein, T., Mikloutz, L., Sidak, K., Plant, C., and Tschiatschek, S. Plasticity loss in deep reinforcement learning: A survey. *arXiv preprint arXiv:2411.04832*, 2024.
- Komatsuzaki, A., Puigcerver, J., Lee-Thorp, J., Ruiz, C. R., Mustafa, B., Ainslie, J., Tay, Y., Dehghani, M., and Houlsby, N. Sparse upcycling: Training mixture-of-experts from dense checkpoints.
- Le Scao, T., Wang, T., Hesslow, D., Bekman, S., Bari, M. S., Biderman, S., Elshahar, H., Muennighoff, N., Phang, J., Press, O., Raffel, C., Sanh, V., Shen, S.,

- Sutawika, L., Tae, J., Yong, Z. X., Launay, J., and Beltagy, I. What language model to train if you have one million GPU hours? pp. 765–782, Abu Dhabi, United Arab Emirates, December 2022. Association for Computational Linguistics. doi: 10.18653/v1/2022.findings-emnlp.54. URL <https://aclanthology.org/2022.findings-emnlp.54>.
- Li, R., Zi, Y., Muennighoff, N., Kocetkov, D., Mou, C., Marone, M., Akiki, C., Jia, L., Chim, J., Liu, Q., et al. Starcoder: may the source be with you! *Transactions on Machine Learning Research*, 2023.
- Liew, S. P., Kato, T., and Takase, S. Scaling laws for up-cycling mixture-of-experts language models. In Singh, A., Fazel, M., Hsu, D., Lacoste-Julien, S., Berkenkamp, F., Maharaj, T., Wagstaff, K., and Zhu, J. (eds.), *Proceedings of the 42nd International Conference on Machine Learning*, volume 267 of *Proceedings of Machine Learning Research*, pp. 37682–37704. PMLR, 13–19 Jul 2025. URL <https://proceedings.mlr.press/v267/liew25a.html>.
- Liu, J., Cui, L., Liu, H., Huang, D., Wang, Y., and Zhang, Y. Logiqa: a challenge dataset for machine reading comprehension with logical reasoning. pp. 3622–3628, 2021.
- Loshchilov, I., Hutter, F., et al. Fixing weight decay regularization in adam. *arXiv preprint arXiv:1711.05101*, 5, 2017.
- Lyle, C., Zheng, Z., Nikishin, E., Pires, B. A., Pascanu, R., and Dabney, W. Understanding plasticity in neural networks. In *International Conference on Machine Learning*, pp. 23190–23211. PMLR, 2023.
- Lyle, C., Zheng, Z., Khetarpal, K., van Hasselt, H., Pascanu, R., Martens, J., and Dabney, W. Disentangling the causes of plasticity loss in neural networks. *arXiv preprint arXiv:2402.18762*, 2024.
- Maloney, A., Roberts, D. A., and Sully, J. A solvable model of neural scaling laws. *arXiv preprint arXiv:2210.16859*, 2022.
- Mandelbrot, B. et al. An informational theory of the statistical structure of language. *Communication theory*, 84(21): 486–502, 1953.
- Mikami, H., Fukumizu, K., Murai, S., Suzuki, S., Kikuchi, Y., Suzuki, T., Maeda, S.-i., and Hayashi, K. A scaling law for syn2real transfer: How much is your pre-training effective? pp. 477–492. Springer, 2022.
- Nikishin, E., Schwarzer, M., D’Oro, P., Bacon, P.-L., and Courville, A. The primacy bias in deep reinforcement learning. In *International conference on machine learning*, pp. 16828–16847. PMLR, 2022.
- Paperno, D., Kruszewski, G., Lazaridou, A., Pham, N.-Q., Bernardi, R., Pezzelle, S., Baroni, M., Boleda, G., and Fernández, R. The lambda dataset: Word prediction requiring a broad discourse context. *Proceedings of the 54th Annual Meeting of the Association for Computational Linguistics (Volume 1: Long Papers)*, pp. 1525–1534, 2016.
- Paquette, E., Paquette, C., Xiao, L., and Pennington, J. 4+3 phases of compute-optimal neural scaling laws. *The Thirty-eighth Annual Conference on Neural Information Processing Systems*, 2024.
- Paster, K., Santos, M. D., Azerbayev, Z., and Ba, J. Openwebmath: An open dataset of high-quality mathematical web text. *arXiv preprint arXiv:2310.06786*, 2023.
- Penedo, G., Kydlíček, H., Lozhkov, A., Mitchell, M., Raffel, C. A., Von Werra, L., Wolf, T., et al. The fineweb datasets: Decanting the web for the finest text data at scale. *Advances in Neural Information Processing Systems*, 37: 30811–30849, 2024.
- Porian, T., Wortsman, M., Jitsev, J., Schmidt, L., and Carmon, Y. Resolving discrepancies in compute-optimal scaling of language models. *Advances in Neural Information Processing Systems*, 37:100535–100570, 2024.
- Que, H., Liu, J., Zhang, G., Zhang, C., Qu, X., Ma, Y., Duan, F., Bai, Z., Wang, J., Zhang, Y., et al. D-cpt law: Domain-specific continual pre-training scaling law for large language models. *Advances in Neural Information Processing Systems*, 37:90318–90354, 2024.
- Sakaguchi, K., Bras, R. L., Bhagavatula, C., and Choi, Y. Winogrande: An adversarial winograd schema challenge at scale. *Communications of the ACM*, 64(9):99–106, 2021.
- Shao, Z., Wang, P., Zhu, Q., Xu, R., Song, J., Bi, X., Zhang, H., Zhang, M., Li, Y., Wu, Y., et al. Deepseekmath: Pushing the limits of mathematical reasoning in open language models. *arXiv preprint arXiv:2402.03300*, 2024.
- Shazeer, N. Glu variants improve transformer. *arXiv preprint arXiv:2002.05202*, 2020.
- Shen, S., Walsh, P., Keutzer, K., Dodge, J., Peters, M., and Beltagy, I. Staged training for transformer language models. In *International Conference on Machine Learning*, pp. 19893–19908. PMLR, 2022.
- Shen, Z., Tao, T., Ma, L., Neiswanger, W., Liu, Z., Wang, H., Tan, B., Hestness, J., Vassilieva, N., Soboleva, D., et al. Slimpajama-dc: Understanding data combinations for llm training. *arXiv preprint arXiv:2309.10818*, 2023.

- Shoeybi, M., Patwary, M., Puri, R., LeGresley, P., Casper, J., and Catanzaro, B. Megatron-lm: Training multi-billion parameter language models using model parallelism. *arXiv preprint arXiv:1909.08053*, 2019.
- Sodhani, S., Chandar, S., and Bengio, Y. Toward training recurrent neural networks for lifelong learning. *Neural computation*, 32(1):1–35, 2020.
- Springer, J. M., Goyal, S., Wen, K., Kumar, T., Yue, X., Maladi, S., Neubig, G., and Raghunathan, A. Overtrained language models are harder to fine-tune. *arXiv preprint arXiv:2503.19206*, 2025.
- Su, J., Ahmed, M., Lu, Y., Pan, S., Bo, W., and Liu, Y. Roformer: Enhanced transformer with rotary position embedding. *Neurocomputing*, 568:127063, 2024.
- Sun, Y., Wang, S., Li, Y., Feng, S., Tian, H., Wu, H., and Wang, H. ERNIE 2.0: A continual pre-training framework for language understanding. In *The Thirty-Fourth AAAI Conference on Artificial Intelligence, AAAI 2020, The Thirty-Second Innovative Applications of Artificial Intelligence Conference, IAAI 2020, The Tenth AAAI Symposium on Educational Advances in Artificial Intelligence, EAAI 2020, New York, NY, USA, February 7-12, 2020*, pp. 8968–8975. AAAI Press, 2020. URL <https://doi.org/10.1609/aaai.v34i05.6428>.
- Tissue, H., Wang, V., and Wang, L. Scaling law with learning rate annealing. *arXiv preprint arXiv:2408.11029*, 2024.
- Touvron, H., Martin, L., Stone, K., Albert, P., Almahairi, A., Babaei, Y., Bashlykov, N., Batra, S., Bhargava, P., Bhosale, S., et al. Llama 2: Open foundation and fine-tuned chat models. *arXiv preprint arXiv:2307.09288*, 2023.
- Vaswani, A., Shazeer, N., Parmar, N., Uszkoreit, J., Jones, L., Gomez, A. N., Kaiser, Ł., and Polosukhin, I. Attention is all you need. *Advances in neural information processing systems*, 30, 2017.
- Wang, P., Panda, R., Hennigen, L. T., Greengard, P., Karlinsky, L., Feris, R., Cox, D. D., Wang, Z., and Kim, Y. Learning to grow pretrained models for efficient transformer training. *arXiv preprint arXiv:2303.00980*, 2023a.
- Wang, X., Tissue, H., Wang, L., Li, L., and Zeng, D. D. Learning dynamics in continual pre-training for large language models. *arXiv preprint arXiv:2505.07796*, 2025.
- Wang, Y., Su, J., Lu, H., Xie, C., Liu, T., Yuan, J., Lin, H., Sun, R., and Yang, H. Lemon: Lossless model expansion, 2023b.
- Welbl, J., Liu, N. F., and Gardner, M. Crowdsourcing multiple choice science questions. *W-NUT 2017*, pp. 94, 2017.
- Yadav, P., Sun, Q., Ding, H., Li, X., Zhang, D., Tan, M., Bhatia, P., Ma, X., Nallapati, R., Ramanathan, M. K., Bansal, M., and Xiang, B. Exploring continual learning for code generation models. In Rogers, A., Boyd-Graber, J. L., and Okazaki, N. (eds.), *Proceedings of the 61st Annual Meeting of the Association for Computational Linguistics (Volume 2: Short Papers), ACL 2023, Toronto, Canada, July 9-14, 2023*, pp. 782–792. Association for Computational Linguistics, 2023. URL <https://doi.org/10.18653/v1/2023.acl-short.68>.
- Yao, Y., Zhang, Z., Li, J., and Wang, Y. Masked structural growth for 2x faster language model pre-training, 2024.
- Zan, D., Chen, B., Yang, D., Lin, Z., Kim, M., Guan, B., Wang, Y., Chen, W., and Lou, J. CERT: continual pre-training on sketches for library-oriented code generation. In Raedt, L. D. (ed.), *Proceedings of the Thirty-First International Joint Conference on Artificial Intelligence, IJCAI 2022, Vienna, Austria, 23-29 July 2022*, pp. 2369–2375. ijcai.org, 2022. URL <https://doi.org/10.24963/ijcai.2022/329>.
- Zhang, B., Liu, Z., Cherry, C., and Firat, O. When scaling meets llm finetuning: The effect of data, model and finetuning method. 2024a.
- Zhang, P., Zeng, G., Wang, T., and Lu, W. Tinyllama: An open-source small language model. *arXiv preprint arXiv:2401.02385*, 2024b.

A. Notations

We summarize main notations used in the paper.

- L : Cross-entropy loss or the (natural) logarithmic loss
- D : Dataset size in token
- N : Non-embedding model size or number of non-embedding parameters
- A, B, F : Scaling factors of the power law, independent of the variable under consideration
- E : Irreducible loss of the power law, independent of the variable under consideration
- α, β, γ : Scaling exponents of the power law, independent of the variable under consideration
- n_{layer} : number of layers of a model
- d_{model} : hidden dimension size of a model
- d_{MLP} : intermediate hidden dimension size of a model

B. More on Architecture and Experimental Design

B.1. Megatron-LM Configuration

Infrastructure. Our experiments are performed on multiple nodes, each consisting of 8 NVIDIA H100 80 GB GPUs, interconnected via InfiniBand HDR. The software we use for training is the Megatron-LM library [Shoeybi et al. \(2019\)](#).

We use and modify the Megatron-LM (core v0.8.0) library for our experiments³. Models are trained with data type bfloat16. Other optimization libraries used include FlashAttention [Dao et al. \(2022\)](#) and TransformerEngine⁴. See the example scripts provided in supplementary material.

B.2. Model Configuration

Let us elaborate more on our model configuration. The intermediate hidden dimension size, d_{MLP} , is set to be four times the hidden dimension size, i.e., $4d_{\text{model}}$. Bias is not used in the linear layers. We do not consider efficiency-motivated implementations like grouped query attention as well. Attention head number is chosen to increase with model size following standard practices. Other designs of the architecture follow Llama2’s closely ([Touvron et al., 2023](#)).

We vary model sizes keeping the ratio $n_{\text{layer}}/d_{\text{model}}$ to lie in the range 32 to 64, as in [Kaplan et al. \(2020\)](#). Smaller models for used for ablation studies. See Table 2 for the exact numbers for the model configuration.

Table 2. Models used in our study and their parametric details. Note that d_{MLP} , is set to be $4d_{\text{model}}$.

Model	n_{layer}	d_{model}	n_{head}	N
15M	9	320	4	14,751,680
44M	12	480	8	44,248,800
0.1B	15	640	8	98,323,840
0.2B	21	832	8	232,623,040
0.5B	26	1,120	16	521,889,760
1B	30	1,504	16	1,085,859,424

B.3. Training Configuration

As discussed in the main text, we adopt the WSD learning rate schedule for all experiments. The number of warmup steps is set approximately equal to the model size, as suggested by [Porian et al. \(2024\)](#). In the final phase of training, the learning rate decays linearly to 10% of its peak value, with the decay phase spanning roughly 10% of the total training steps, following the setup in [Hägele et al. \(2024\)](#). To emulate varying token budgets, we save intermediate checkpoints at logarithmically spaced intervals.

The general training configuration is summarized in Table 3, while model-specific hyperparameters, such as warmup

³<https://github.com/NVIDIA/Megatron-LM>

⁴<https://github.com/NVIDIA/TransformerEngine>

Table 3. Training configuration used throughout the paper.

Configuration	Details
Context length	1,024
Embedding tying	False
Optimizer	AdamW Loshchilov et al. (2017)
Adam β_1	0.9
Adam β_2	0.95
Adam ϵ	1e-8
Weight decay	0.1
Gradient clipping	1.0

iterations, initialization standard deviation ($\sqrt{2/5d_{\text{model}}}$ (Le Scao et al., 2022)), maximum training steps, batch size, and tuned learning rate, are provided in Table 4. Batch size is scaled with model size according to standard practice, without tuning for optimality. The number of tokens is increased with model size as well, such that the parameter-to-token ratio remains roughly constant across different model sizes. We note that no specialized techniques for mitigating training instabilities, such as Z-loss or QK normalization, are employed, as such instabilities do not arise in our experiments.

Table 4. Model-dependent training configuration. "init. size" refers to the standard deviation of the normal distribution used for initializing the weights. "Std iter." refers to the number of iteration run on the model to reach about 70 times the model size in tokens, the standard training length used in the scaling law experiments. For several models, we also run longer training for exploration.

Model	warmup iter.	init. size	Std iter.	batch size	LR
15M	200	0.035	17,600	128	8e-3
44M	200	0.029	17,600	256	4e-3
0.1B	200	0.025	17,600	512	4e-3
0.2B	400	0.022	35,200	512	2e-3
0.5B	800	0.019	70,400	512	4e-4
1B	800	0.016	70,400	1024	4e-4

B.4. On the choice of Data Domains Studied

Here, we argue that our experimental setup for CPT incorporates a significant domain shift, and it is highly relevant to frontier model research.

- **Domain gap in our setup.** The base models are purposefully pretrained exclusively on the Common Crawl portion of the Slimpajama-DC dataset. This explicitly excludes data heavily skewed toward specialized domains such as mathematics (like arXiv) or code (like dedicated GitHub repositories), thereby maximizing the domain gap for the subsequent CPT stage.
- **Small overlap of domains.** While some minimal token overlap between the generic web corpus and the specialized domains is inevitable, it is quantitatively small. We estimate that math/code data accounts for approximately 0.3 percent of the total Slimpajama-DC corpus.⁵ Consequently, the domain shift in our CPT experiments, which move to dedicated code and math corpora, is substantial.
- **Relevance to frontier LLM training.** The strategy of pretraining mainly on generic web data and subsequently applying CPT on specialized domains like code (Stack/StarCoder) and mathematics (OpenWebMath) is a standard and highly relevant practice for state-of-the-art LLMs.
- **Model growth.** For model growth experiments, the primary goal is to isolate and quantify the effect of increasing model capacity, not domain shift. Therefore, the second stage is intentionally conducted on the same generic web dataset as the base model, allowing us to accurately quantify the scaling behavior of the growth technique itself.

⁵Estimated based on filtering performed for the OpenCoder (Huang et al., 2025) dataset, which extracted math/code data from a similar CommonCrawl-derived corpus, FineWeb (Penedo et al., 2024).

To summarize, our current findings are robust within the most practically relevant and challenging domain-transfer scenarios currently employed for large-scale LLM training.

B.5. GPU Hours and Costs

Instead of reporting the actual runtimes on our cluster, which varied in our experiments due to many factors affecting the cluster (number of available nodes, congestion, etc.), we give a theoretical estimate of total GPU hours used for obtaining the joint scaling law, which involves running the largest tested model with most training tokens in this paper.

The estimate is as follows. We calculate the FLOPs for training the largest first and second-stage models with maximum iterations using the $6ND$ approximation, ignoring the additional FLOPs required to continued pretrain models with shorter iterations (as we can reuse the intermediate checkpoints).⁶ We further assume that the per-second TFLOPs of the GPU is 400. We obtain around 10^9 TFLOPs. Taking into account of additional experimentation and ablation runs, we estimate that around 3000 GPU hours were used for the entire project. Assuming a cost of 2 USD per GPU hour, the total cost is around 10,000 USD.

Scaling law methodology and cost justification. We note that our study contains over 450 total runs, as accurately mapping the relationship between multiple scaling variables (model size N , first-stage tokens D_1 , and second-stage tokens D_2) necessitates a multitude of controlled experiments on models of various sizes. This methodology contrasts with single, large-scale training runs (e.g., training one 7B model from scratch), which would provide fewer data points for fitting complex scaling laws. This rigorous approach, balanced with the need for a reasonable overall budget, dictates our focus on models up to 1B parameters for extensive experimentation.

C. Training Details

C.1. Ablation of Learning Rate Schedules

Here, we compare the performances of using WSD and the commonly used learning rate (LR) cosine schedules (decaying to 10% of the peak LR value) (Touvron et al., 2023). The model size we use is 0.1B, with the following training configuration: batch size 512, 4,000 training iterations, and 200 warmup iterations. We can see from Figure 5 that both schedules yield similar (with WSD achieving slightly better final loss) performances. This justifies our choice of using the WSD schedule throughout the paper.

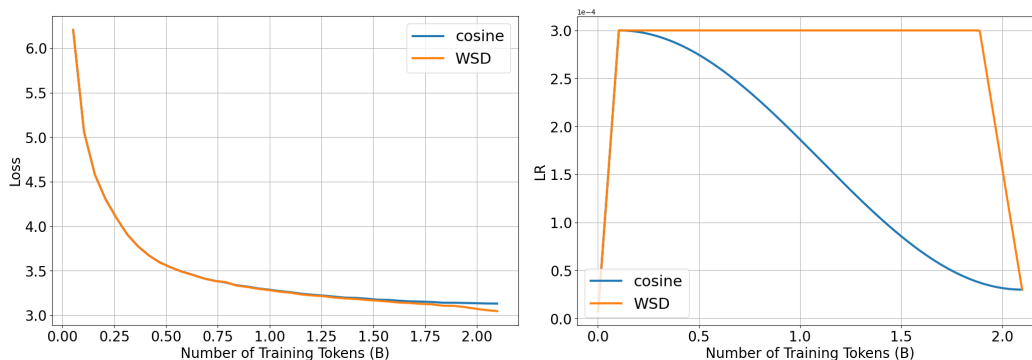


Figure 5. **WSD vs cosine LR schedule.** We show that the WSD LR schedule achieves similar (even slightly better) final loss compared to the more commonly used cosine LR schedule.

C.2. Ablation of Data Repetition

During model growth, we have used the same data as the base model for the second stage of training. This is because the base model is often trained with a large amount of data, and it is not always possible to obtain a large amount of additional data. However, this means that the second stage of training involves repeating the same data. To study the effect of data

⁶We have more than 450 runs; estimated from 25 data points for each of the 8 methods considered in Table 1, and 125 data points for the two joint scaling law experiments (CPT and model growth).

repetition, we have made an ablation study, where we compare the performance of using the same data as the base model and using different portion of the Slimpajama data. As shown in Figure 6, we find that the difference is small.

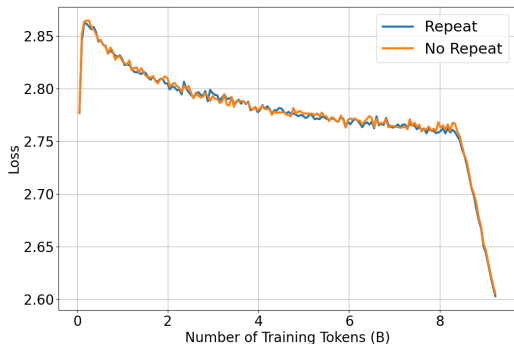


Figure 6. **Ablation of data repetition during model growth.** We compare the performance of using the same data as the base model and using different data for the second stage of training. The difference is small, indicating that data repetition does not affect the scaling behavior significantly.

C.3. Evaluation with Standard Benchmarks

We compare the performance of our trained 1B base model against existing models with similar sizes, Pythia (Biderman et al., 2023) and TinyLlama (Zhang et al., 2024b), based on standard natural language processing benchmarks, ARC (Clark et al., 2018), lambada (Paperno et al., 2016), logiqa (Liu et al., 2021), piqa (Bisk et al., 2020), sciq (Welbl et al., 2017), and winogrande (Sakaguchi et al., 2021).

Table 5 shows the results. We see that the model perform similarly to the open models, indicating that our models have been trained correctly.

Table 5. **Benchmarks’ performance comparison across models.** Reported scores are accuracies (normalized by byte length whenever applicable). The first two columns are scores of existing models. The last column is evaluation results of the largest base model trained with the most number of tokens in this work. Our models are evaluated with the LM Evaluation Harness v0.4.0 library (Gao et al., 2024).

Models	Pythia-1B	TinyLlama-1.1B	Our 1B model
Datasets	Pile	Slimpajama & Starcoder	Slimpajama
Tokens	100B	103B	74B
ARC-c	25.59	24.32	27.65
ARC-e	47.26	44.91	52.10
lambada	53.52	-	45.08
logiqa	29.49	-	26.11
piqa	69.31	67.30	65.89
sciq	77.3	-	78.10
winogrande	51.22	53.28	54.93
Avg.	50.53	-	49.98

C.4. Continual Pretraining Details

Using a lower LR for CPT is also a common practice (Ibrahim et al., 2024). As an ablation, we have experimented with using a constant LR schedule setting the value to be the final LR for the first-stage base model training, on a 0.1B model. We find that it yields worse performance (see Figure 7). Hence, we use the same LR (and LR schedule) as the base model for CPT.

C.5. Model Growth Details

For completeness, we provide more details on the model growth methods used in this work.

Width expansion details. Let us elaborate more on the width expansion method used in this work. We first give a more precise definition of function preservation. Let F be a function and G as the growth operator. The function preservation condition is defined as:

$$F(x) = G(F)(x), \forall x \in \mathcal{X}$$

where \mathcal{X} is the input space.

When performing width expansion, the neuron values of each layer are expanded by duplicating the weights of existing neurons, and dividing the output weights by the growth factor.

Stacking details. We first note that stacking does not preserve function but is empirically found to work well in practice (Du et al., 2024). We use the recommended stacking procedure in Du et al. (2024), which is, letting M be the non-embedding part of the base model, the stacked model with growth factor k is given by:

$$M' = M \circ M \circ \dots \circ M \quad (k \text{ times})$$

where \circ denotes function composition. The embedding and final layer are then simply copied from the base model.

Low LR. We also experiment with using a lower constant LR for stacking as above, and find that it also yields worse performance (see Figure 7). Hence, we use the same LR (and LR schedule) as the base model for stacking as well.

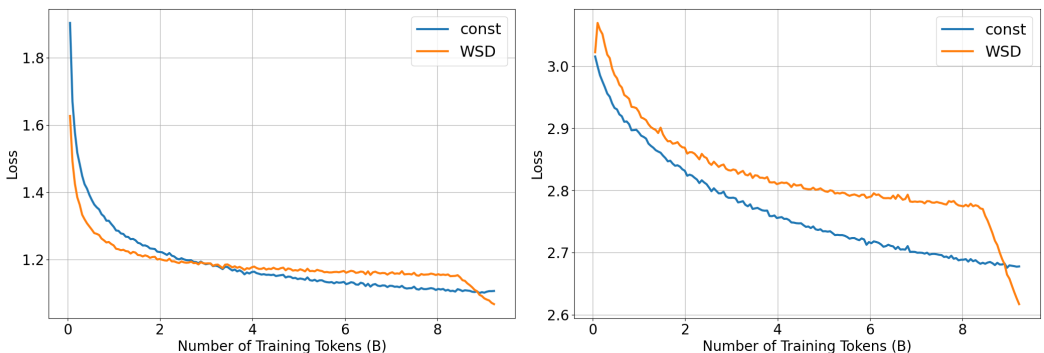


Figure 7. **model reuse with lower LR.** We show that using the same LR as the base model achieves better final performance than using a lower LR for a 0.1B model continual pretrained on code data (left) and stacking (right).

D. Scaling Laws Details

D.1. Fitted Exponents and Other Results

We show the fitted exponents of the multiplicative scaling laws studied in Table 1 in Table 6.

We further show that D_1 has power-law scaling in Figure 8, for CPT on mathematics data and model growth by expansion, which justifies the multiplicative form of the scaling laws.

D.2. Another variant of CPT scaling law.

When the dataset used for CPT is the same as the base model, we expect the following continuous scaling formula shown below holds:

$$L(D_1, D_2) = A(D_1 + D_2)^{-\alpha} + E \tag{11}$$

Hence, one may expect this holds for CPT on a different dataset as well, as assumed in Que et al. (2024); Wang et al. (2025). Fitting the above formula for the code (math) CPT scenario, we find that the RMS error is 0.0213 (0.0235), higher than the best ones in Table 1. Hence, our scaling law models CPT better, in contrast to previous assumptions, which may have overlooked the discontinuous (overtraining) effects of CPT.

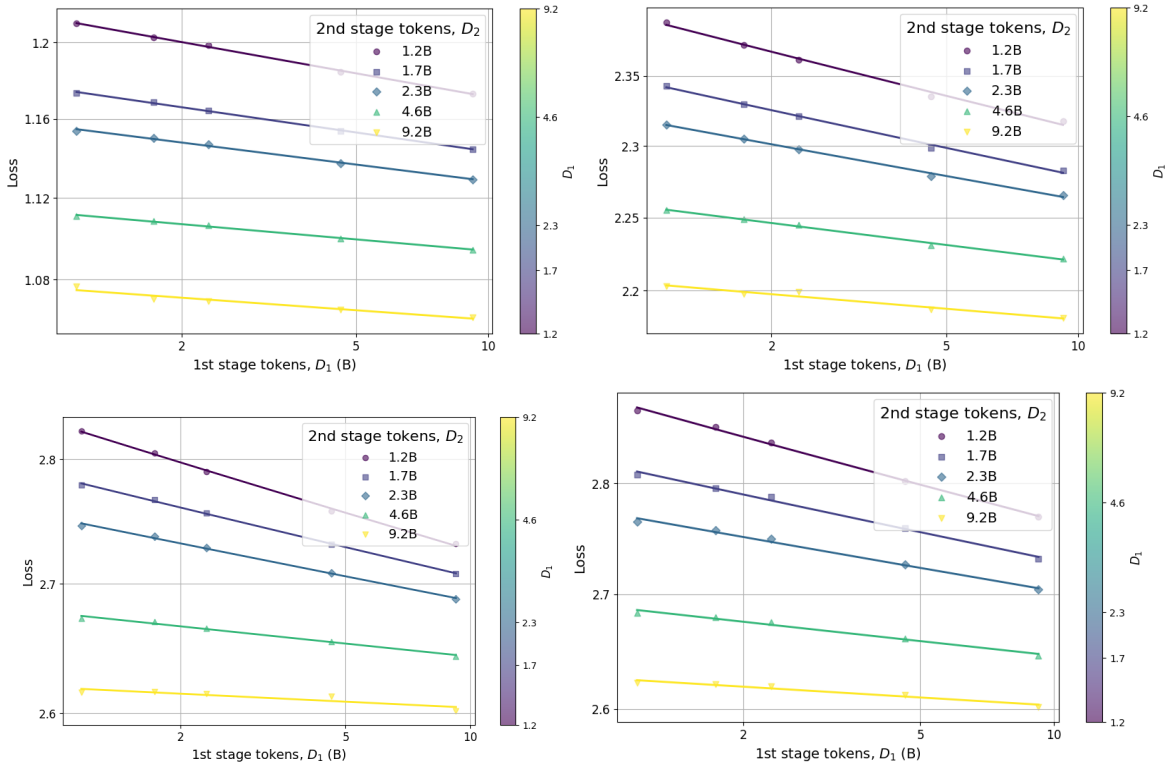


Figure 8. D_1 has power-law scaling. We show scaling behavior of first-stage training tokens (D_1) for different values of second-stage tokens (D_2), indicating that D_1 also has power-law scaling. **Top left:** Continual pretraining on code. **Top right:** Continual pretraining on mathematics data. **Bottom left:** Model growth by stacking (growth factor 2). **Bottom right:** Model growth by expansion (growth factor 2).

One may further wonder if the model growth methods follow the above scaling law, since both stages use the same dataset. However, we find that the RMS error for (growth factor 2) expansion and stacking methods are 0.032 and 0.025 respectively, again larger than the ones in Table 1. Even though the same dataset is used in training, the model capacity is changed in model growth, explaining why the continuous scaling law does not hold. In Figure 9, we show that the continuous scaling law does not fit the data well visually.

D.3. Joint Scaling Law

For model growth, we also fit the joint scaling law in Equation 9. Note that there is ambiguity in defining the model size N in the context of model growth. We consider N to be the size of the model before growth, and as we keep the growth factor fixed to be 2 in our experiments, the new model size after growth is $N' = 2N$. Therefore, N and N' differ by a constant factor of 2, which can be absorbed into the coefficient B in Equation 9. Unless stated otherwise, we use N in the fitting of the joint scaling law for model growth. In Figure 9, we show the fit of the joint scaling law for stacking.

We provide the fitted coefficients of the joint scaling law in Table 7. In addition to model reuse, we also show the fitted coefficients for base models trained from scratch on the same dataset as the second stage (code data for CPT, and the same data as the base model for model growth). For model growth, we consider a growth factor of 2, and fit the parameters with model size N before stacking for comparison conveniences. We further note that the fitted coefficients are produced by fitting the joint scaling law to *all* data points collected, including those used for validation in Figure 9.

D.4. Why Fitting Scaling Laws Separately?

We justify our decision to fit two separate scaling laws—one for models trained from scratch and another for model reuse—instead of employing a unified formulation that spans all stages.

Table 6. **Fitted exponents for the multiplicative scaling law.** Corresponding $\alpha_1, \alpha_2, \alpha_3$ values for the multiplicative interaction fits shown in Table 6.

Variant	α_1	α_2	α_3
CPT (code)	0.106	0.146	0.004
CPT (math)	0.981	0.388	0.017
Expand	0.549	0.852	0.024
Stack	0.515	0.350	0.017
CPT (replay)	0.424	0.626	0.018
CPT (stable)	0.920	0.156	0.004
Stack (x4)	0.644	0.829	0.028
Stack (stable)	0.891	0.507	0.009

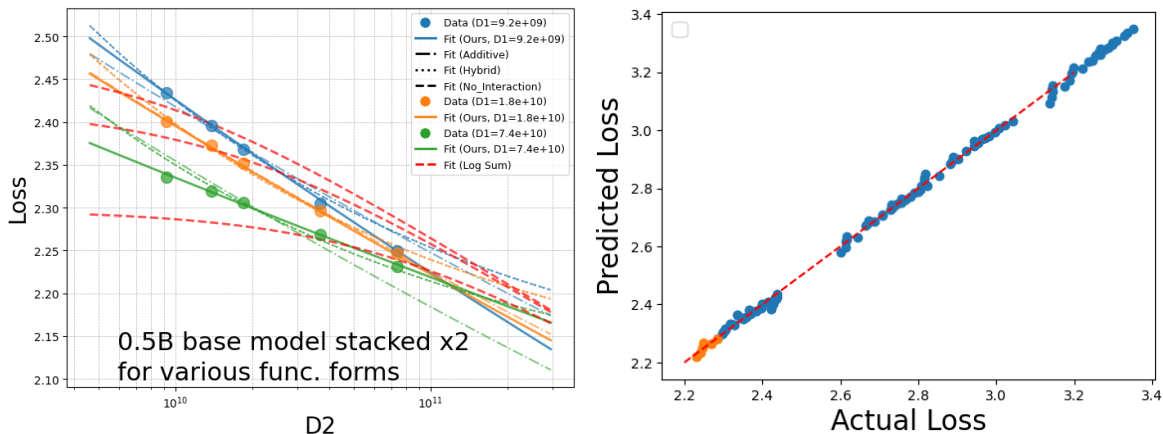


Figure 9. **Left: Fits with different functional forms.** We show in red the fits of the continuous scaling law does not capture the saturation effect well compared to our proposed multiplicative scaling law. **Right: Fits of the joint upcycling scaling law of stacking.** 10% of the collected data points with lowest losses are used for validation (orange points).

First, the scaling behavior of models trained from scratch is expected to differ from that of models undergoing second-stage pretraining. Specifically, at the limit $D_1 \rightarrow 0$, grown models are initialized from a pretrained base model, whereas scratch-trained models start from random weights. This difference in initialization leads to distinct learning dynamics and, consequently, different scaling law parameters.

Similarly, the scaling behavior of the base model differs from that of the second-stage training in the limit $D_2 \rightarrow 0$. As shown in Figure 7, second-stage training often begins with a *rearming* phase, during which the loss initially increases before decreasing. This early instability deviates from the expected scaling of dense models, although the overall trend remains correlated—supporting the validity of Condition 1, due to function preservation and empirical observations that rearming does not entirely disrupt loss behavior (as quoted from Clauzet et al. (2009): “In practice, few empirical phenomena obey power laws for all values of x ”).

Finally, our preliminary experiments indicate that a unified scaling law does not provide a satisfactory fit across both stages. We therefore opt to model them separately. We also note that there may exist alternative functional forms that could better capture the full range of behavior, but they may violate some of the well-established conditions for scaling laws (power law), and may overcomplicate the analysis or overfit the data; hence, we leave their exploration to future work.

E. More Observations and Implications of the Scaling Laws

E.1. Implication based on Scaling Laws’ Extrapolation

We consider an implication based on the extrapolation of the scaling laws, motivated by studies on MoE upcycling (Komatsuzaki et al.; Liew et al., 2025).

Table 7. **Fitted coefficients for joint scaling laws.** Note that for stacked models, we fit the coefficients with model size N before stacking for comparison conveniences.

	α/α_1	α_2	α_3	β	A	B	E
Base (Sлимпajama)	0.092	-	-	0.105	10.383	10.085	0.041
From-scratch (code)	0.113	-	-	0.234	8.143	27.286	0.105
CPT (code)	0.048	0.126	0.001	0.238	15.062	27.234	0.105
Stack	0.087	0.119	0.003	0.173	33.394	22.471	0.041

A key practical consideration is how much of the *initial investment* in pretraining, the so-called *sunk cost* (D_1), can be effectively leveraged in the second stage of training. This question has been explored in the context of MoE upcycling strategies. For example, it was found that upcycling yields benefits up to 120% of the sunk cost. That is, to match the performance of an upcycled MoE model that underwent an additional 0.4 trillion tokens of training after an initial 2T tokens, training a comparable MoE from scratch would require 2.4T tokens—representing an effective saving of 2T tokens.

We investigate this in model growth by stacking (growth factor 2). We define D^* as the number of tokens required for training from scratch to match the performance of a grown model with the same sunk cost, following Liew et al. (2025):

$$L_{2N}^{\text{scratch}}(D^*) = L_N^{\text{grown}}(D_1 = D^*, D_2 = D^*) \quad (12)$$

where $L_{2N}^{\text{scratch}}(D)$ is the loss of a model of size $2N$ trained from scratch for D tokens, and $L_N^{\text{grown}}(D_1, D_2)$ is the loss of a model of size $2N$ grown from a base model of size N trained for D_1 tokens, and then trained for D_2 tokens. To obtain $L_{2N}^{\text{scratch}}(D)$, we fit the losses of models trained from scratch with the Chinchilla-style scaling law (see Table 7 in Appendix D.3 for the fitted coefficients).

The right panel of Figure 10 shows that D^* decreases with increasing model size, with D^* equal to 13T tokens for a 100B model. When $D_2 \lesssim D^*$, the required from-scratch tokens to catch up is more than 100% of D_1 : model growth remains more efficient than training from scratch. However, beyond this threshold, from-scratch training becomes more efficient. Solving Equation 12, we can approximate the threshold D^* analytically as $D^* \simeq 13 \left(\frac{N}{10^{11}}\right)^{-0.6-0.04 \log(N/10^{11})}$ T tokens.

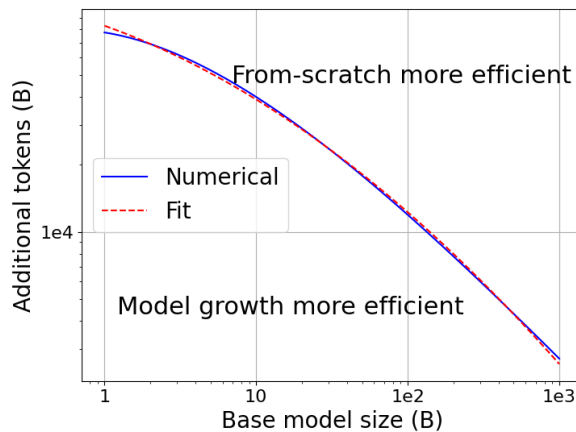


Figure 10. **Model growth efficiency decreases with sunk cost and model size.** For token budgets above the curve(s), training from scratch is more efficient than stacking-based model growth (growth factor 2); for budgets below, model growth remains advantageous. Shown are the numerical (blue) and analytical (red) solutions of Equation 12. Vertical axis is D^* as in Equation 12.

E.2. Compute Optimality

For scaling studies of LLMs, the cost of training is often estimated using floating point operations (FLOPs), which we simply refer to as compute. The compute cost can be approximated as $C = 6ND$ (Kaplan et al., 2020). One is often

interested in training LLMs with the least amount of compute. For CPT, optimizing the compute based on Equation 6 leads to the scaling relations:

$$D_2^{\text{opt}} \propto C_2^{\frac{\beta}{\beta + \alpha_{\text{eff}}}}, \quad N_1^{\text{opt}} \propto C_2^{\frac{\alpha_{\text{eff}}}{\beta + \alpha_{\text{eff}}}} \quad (13)$$

where $\alpha_{\text{eff}} := \alpha_2 - \alpha_3 \log D_1$. Notably, as D_1 increases, α_{eff} decreases, meaning larger models require more tokens for compute-optimal model reuse.

For model growth with growth factor 2, we want to scale N_2, D_2 optimally, $N_2^{\text{opt}}, D_2^{\text{opt}}$, given a FLOPs budget and fixing D_1 , while minimizing the loss L , which we write as $L_{D_1}(D_2, N_1)$. Here, N_1 is the model size before growth, and $N_2 = 2N_1$. This is equivalent to solving the following:

$$\begin{aligned} \frac{\partial}{\partial D_2} L_{D_1}(D_2, C_2/12D_2) \Big|_{D_2=D_2^{\text{opt}}} &= 0, \\ \frac{\partial}{\partial N_1} L_{D_1}(C_2/12N_1, N_1) \Big|_{N_1=N_1^{\text{opt}}} &= 0 \end{aligned}$$

where we have used $N_2 = 2N_1$ and $C_2 = 6N_2D_2$. Solving the above equations leads to

$$\begin{aligned} D_2^{\text{opt}} &= G \left(\frac{C_2}{12} \right)^a, \\ N_1^{\text{opt}} &= G^{-1} \left(\frac{C_2}{12} \right)^b \end{aligned}$$

where

$$\begin{aligned} G &:= \left(\frac{A_{\text{eff}} \alpha_{\text{eff}}}{B \beta} \right)^{1/(\alpha_{\text{eff}} + \beta)} \\ a &:= \frac{\beta}{\alpha_{\text{eff}} + \beta} \\ b &:= \frac{\alpha_{\text{eff}}}{\alpha_{\text{eff}} + \beta} \\ A_{\text{eff}} &:= A D_1^{-\alpha_1} \\ \alpha_{\text{eff}} &:= \alpha_2 - \alpha_3 \log D_1 \end{aligned}$$

We can henceforth relate D_2^{opt} and N_1^{opt} via

$$D_2^{\text{opt}} = G (G N_1^{\text{opt}})^{a/b} \propto (N_1^{\text{opt}})^{\beta/\alpha_2 - \alpha_3 \log D_1}$$

and

$$N_1^{\text{opt}} = G^{-1} (G^{-1} D_2^{\text{opt}})^{b/a} \propto (D_2^{\text{opt}})^{(\alpha_2 - \alpha_3 \log D_1)/\beta}$$

Notably, as D_1 increases, α_{eff} decreases, meaning larger models require more tokens for compute-optimal model reuse. We leave empirical verification of these relationships to future work, primarily due to cost considerations (see Appendix B.5 for an estimate of GPU hours spent in the work).

E.3. Training with Extremely Large second-stage Token-to-Parameter Ratio

15M-to-30M model. We show the loss values of the last three D_2 points (each run with different D_1 's) in Table 8. To estimate the stochastic noise on the loss, for each D_2 , we train again from the nearest stable-phase checkpoint but with three different random seeds. Although there is slight indication of crossover (comparing $D_1 = 0.2884, 9.2275$ at $D_2 = 9.2275, 27.6824$), we are unable to make strong claims on it without a better understanding of the noise effects.

0.5B-to-1B model. We also train the larger 0.5B-to-1B model to more extreme token-to-parameter ratios (up to 200). The result is shown in Figure 11 (and Table 9 for the last four measured D_2), where we do not see significant crossover at the large D_2 limit.

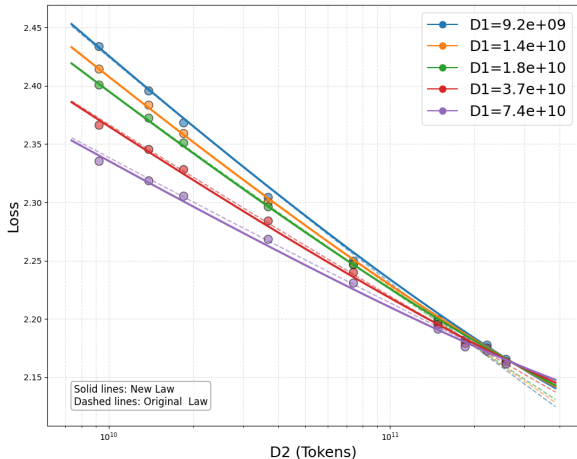


Figure 11. Stacking with extremely large token-to-parameter ratio (0.5B-to-1B). We compare the original scaling law and the new scaling law with a new fitting parameter $D_{2,max}$.

Furthermore, at large D_2 , the points are slightly curved upwards. This can best be seen by modifying the scaling law using a similar argument given in Section 4.2, by adding a new fitting parameter $D_{2,max}$:

$$\hat{D}_2 = (D_2^{-1} + D_{2,max}^{-1})^{-1}, \tag{14}$$

The mean square error of the "tail" for the original and new scaling law are 2.7e-5 and 1.3e-5 (with similar global mean square errors) indicating that the new one fits the tail better (and from the Figure the new scaling law has an upward curve at large D_2). This new formulation predicts a crossover and saturation of the curves afterwards (crossover occurs only when the fitted $D_{2,max} \lesssim e^{\alpha_2/\alpha_3}$). The predicted crossover is beyond the computational reach and is in the region where noises are dominant.

Table 8. 15M-to-30M models' cross-entropy losses and the estimated error from multiple runs with different random seeds.

D_2 (B)	D_1 (B)	Loss	Error
9.2275	0.2884	3.069959	± 0.001345
	0.4325	3.069911	
	0.5767	3.078497	
	1.1534	3.068825	
	2.3069	3.070050	
	9.2275	3.073884	
18.4549	0.2884	3.055554	± 0.004026
	1.1534	3.065518	
	2.3069	3.060454	
	9.2275	3.063905	
27.6824	0.2884	3.055849	± 0.005699
	1.1534	3.053557	
	2.3069	3.051366	
	9.2275	3.054023	

E.4. More on Mechanistic Explanations

We show the gradient norms of model growth by stacking in Figure 12, where we also see that the gradient norms decrease with D_1 for fixed D_2 , indicating saturation effects.

Table 9. 0.5B-to-1B models’ cross-entropy losses. The estimated error is 0.0012-0.0016.

D_2 (B)	D_1 (B)	Loss
147.6395	9.2275	2.199658
	18.4549	2.198132
	36.9099	2.195471
	73.8198	2.191318
184.5494	9.2275	2.182314
	36.9099	2.179196
	73.8198	2.176350
221.4593	9.2275	2.178030
	36.9099	2.175260
	73.8198	2.172848
258.3691	9.2275	2.165875
	36.9099	2.163731
	73.8198	2.161603
258.3691	9.2275	2.165875
	36.9099	2.163731
	73.8198	2.161603

Next, we study other possible mechanistic explanations of the saturation effects. Our scope of investigation is inspired by Lyle et al. (2023; 2024); Klein et al. (2024), which studied mechanistic signatures of plasticity loss in continual learning.

Parameter norms. Increased parameter norms (or weight norms) are indicated to be a signature of plasticity loss (Nikishin et al., 2022). However, as in Figure 13, we do not observe a clear trend of parameter norms with D_1 (which correlates directly with saturation) when training our models. See the caption of Figure 13 for more details.

Sharpness via training trajectory. Lyle et al. (2023) suggested to look at the variance of training curves as a proxy for sharpness, i.e., increased variance in the training curves indicates that it is harder for the model to navigate the sharper loss landscape, indicating plasticity loss. As in Figure 14, we do not observe a clear trend of difference in variance of training curves for different values of D_1 either (except in early training where training with smaller D_1 has slightly lower variance). See the caption of Figure 14 for more details.

Sharpness via Hessian. Another way of studying the loss landscape is through the top eigenvalue of the Hessian (λ_{max}). Here, we present a preliminary analysis using this quantity. We use the Hessian-vector-product and power iteration to estimate λ_{max} on training samples using base models trained with different D_1 . In Figure 15, we show the estimated λ_{max} with respect to D_1 .

The overall trend is not very clear, but roughly speaking, we see that the model reuse scenarios (CPT on code, math; stacking) have some correlation with D_1 , while training with the same data does not seem to correlate with D_1 .

To summarize, we only observe a clear trend of gradient norms with D_1 among the mechanistic quantities studied. We leave the studies of other possible mechanisms (and a more detailed study of the Hessian) to future work.

E.5. More on the Toy Model

Theoretical derivation of the exponential distribution w.r.t. depth. The exponential decay of probability with respect to depth d is a derivation from the maximum entropy principle motivated by Mandelbrot’s work on the distribution of word frequencies (Mandelbrot et al., 1953).

We seek a probability distribution $P(d)$ that maximizes Shannon Entropy $H = - \sum P(d) \ln P(d)$ subject to normalization

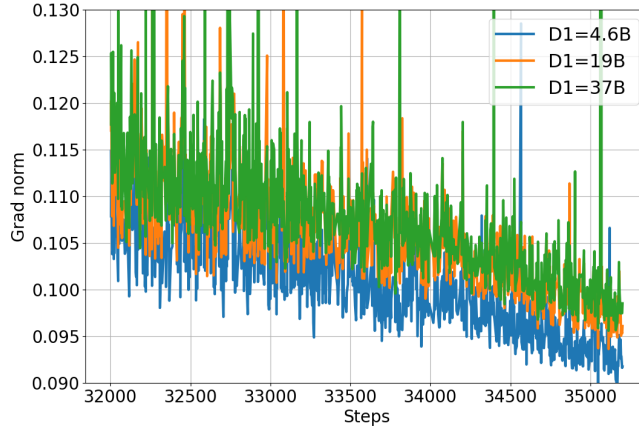


Figure 12. **Overtrained models have larger gradient norms when undergoing model reuse.** We show the gradient norm curves for model growth (0.5B to 1B model via stacking) with respect to number of training steps in the second stage for base models trained with different values of first-stage tokens (D_1).

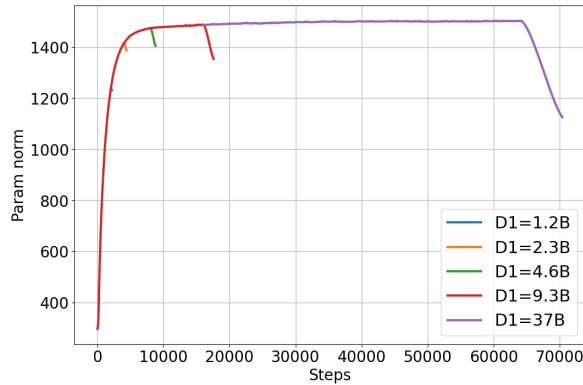


Figure 13. **Parameter norms do not show clear trend with D_1 .** We show the parameter norm curves training a 0.1B base model with respect to number of training steps, where the end of each line corresponds to the parameter norm of a base model trained with the respective number of training steps, D_1 . The parameter norms of models (of various D_1) we use increase before decreasing with respect to D_1 (i.e., non-monotonic). There is therefore no direct correlation with D_1 (which correlates directly with saturation).

$\sum P(d) = 1$ and a fixed average cost $\sum P(d)C(d) = \bar{C}$. Using Lagrange multipliers:

$$L = - \sum P(d) \ln P(d) - \lambda_0 \left(\sum P(d) - 1 \right) - \lambda \left(\sum P(d)C(d) - \bar{C} \right)$$

Setting $\frac{\partial L}{\partial P(d)} = 0$ solving for $P(d)$ yields the exponential (Boltzmann) distribution:

$$P(d) \propto e^{-\lambda \cdot C(d)}$$

In our tree model, depth d represents the search cost C . This decay results in the power-law distribution of features.

More on Hutter’s learning curve theory. Let us describe the setup of [Hutter \(2021\)](#) in more detail: Each datum is associated with a feature k , and the feature is memorized when it is observed during training. Assuming that i.i.d. data are drawn from a distribution $P(k)$, the expected loss is then proportional to the probability of encountering an unobserved feature during training after D training samples:

$$L \propto \sum_{k=1}^{\infty} P(k) (1 - P(k))^D$$

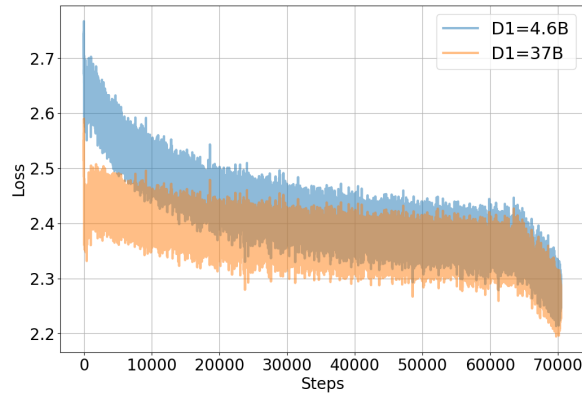


Figure 14. **Variance of training curves do not show clear trend with D_1 .** We show the variance of training curves for model growth by stacking (0.5B to 1B) with respect to number of training steps in the second stage for base models trained with different values of first-stage tokens (D_1). Up to 10,000 steps, the variance is slightly smaller for the training curve with lower D_1 . However, there is no clear trend of variance in the training curves for different D_1 onwards.

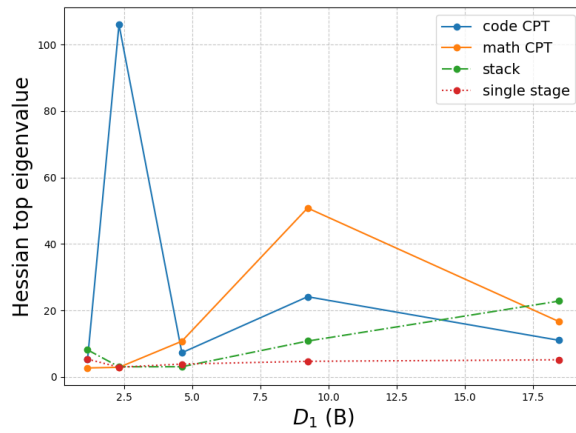


Figure 15. **Hessian with respect to D_1 .** We show the Hessian (λ_{max}) of a 0.1B model base models trained with different values of first-stage tokens (D_1), on model reuse scenarios (CPT on code, math; stacking) and single-stage training scenario. The number of power iteration in calculating λ_{max} is 10, and the number of samples used to test each scenario is 128.

Reusing Overtrained Language Models Saturates Scaling

If $P(k)$ follows a power-law distribution $P(k) \sim k^{-(1+\alpha)}$, the loss can be shown to scale as $L \sim D^{-\alpha/(1+\alpha)} \approx D^{-\alpha}$ for small α .

Note that a simpler alternative assumption that leads to the same conclusion at small α is that features at the tail of the feature distribution is simply not observed during training. The loss is then an integral over the tail:

$$L = \int_D^\infty k^{-(1+\alpha)} dk \sim D^{-\alpha},$$

leading to the same scaling behavior.